

RESOLVENT ANALYSIS OF TRANSITIONAL AND TURBULENT FLOWS AROUND AIRFOILS FOR TRAILING-EDGE NOISE MODEL

S. Demange and K. Oberleithner
Laboratory for Flow Instabilities and Dynamics
Technische Universität Berlin
Contact: s.demange@tu-berlin.de

Z. Yuan and A. Hanifi
FLOW
Department of Engineering Mechanics
KTH Royal Institute of Technology

A. V. G. Cavalieri
Divisao de Engenharia Aeronáutica
Instituto Tecnológico de Aeronáutica

ABSTRACT

We present the results of a physics-based model of the trailing-edge noise radiated by a NACA0012 airfoil at low angle of attack, obtained from resolvent analysis of the turbulent mean flow. Most aeroacoustic models require turbulent spectra of surface pressure fluctuations to reconstruct the acoustic field, which are often derived from empirical models. In our approach, the acoustic model input is reduced to the optimal coherent structures identified by the resolvent. This method has the advantage of isolating the main mechanisms generating noise in the turbulent flow and, unlike empirical models, is applicable to a wide variety of cases.

The model is evaluated for two different configurations: (i) an airfoil with a smooth surface at transitional Reynolds number ($Re = 5.10^4$), resulting in *tonal* noise; and (ii) the same airfoil with a zigzag trip near the leading edge at higher Reynolds number ($Re = 2.10^5$), resulting in *broadband* noise. Large eddy simulations (LES) were performed for both cases to obtain the mean flow, which is used to construct the linear operator underlying the resolvent analysis. A spectral proper orthogonal decomposition (SPOD) of the LES snapshots was used to extract the main hydrodynamic and acoustic features of the flow, which served as a reference for the physics-based model.

Results for the tonal case show an excellent agreement between the resolvent and the SPOD modes at the frequency of the main tones in terms of dominant coherent structures and acoustic directivity. For the broadband case, a good agreement is also obtained for $St < 10$, where low-rank dynamics are identified by the SPOD. This match is improved when considering a simple model of eddy viscosity in the resolvent, and even small changes to the mode shapes have a visible influence on the acoustic directivity. This suggests that a resolvent-based model could be a valuable tool in optimisation methods for the control of trailing-edge noise.

1 Introduction

Airfoil trailing edge (TE) noise is a significant contributor to noise pollution produced by airfoils in uniform flow, which severely limits the development of industrial applications such as onshore wind turbines. Thus, improving the accuracy of low-order TE noise models that can be integrated into optimisation methodologies is an active research topic in the aeroa-

coustics community.

Following the work of Lighthill (1952) on the scattering of pressure fluctuations in the vicinity of a sharp edge, a number of aeroacoustic models have been developed to deal with trailing edge noise. A recent review of these is provided by Lee *et al.* (2021). However, most of these models rely on empirical or semi-empirical models of surface pressure fluctuations for turbulent flows, derived from experimental datasets. Although these models are computationally efficient, they do not reveal the underlying mechanisms of pressure fluctuations, and their accuracy decreases as the cases studied differ from the dataset from which they were derived. Therefore, it is challenging to estimate *a priori* how noise reduction techniques that modify the flow field will impact these models (Lee *et al.*, 2021), and a physics-based method is advisable instead.

Linearised mean flow analyses have been extensively used in recent years to extract coherent structures from turbulent flows, in particular with the development of the resolvent methodology proposed by McKeon & Sharma (2010). Coherent structures from the flow around airfoils were recently analysed with a global resolvent analysis (Ricciardi *et al.*, 2022) and showed promising comparison against results from non-linear simulations.

In the present work, we consider spanwise-coherent structures and acoustic fields, following Nogueira *et al.* (2017), who showed that surface pressure fluctuations with a zero spanwise-wavenumber are efficiently radiated into the acoustic field for all frequencies. Therefore, we use a two-dimensional resolvent analysis of the turbulent spanwise-time-averaged flow to extract the surface pressure fluctuations injected into a closed form of Lighthill's acoustic analogy derived by Curle (1955). However, it should be noted that the independent preliminary attempt of Wagner & Sandberg (2020) in a similar method is limited to a single frequency and a lower Reynolds number.

2 LES datasets

We consider a NACA0012 profile with unit chord length c in a uniform flow characterised by its Reynolds number $Re = \rho_\infty u_\infty c / \mu_\infty$, where ρ_∞ , u_∞ , and μ_∞ denote respectively the density, velocity, and viscosity of the fluid in the freestream, and Mach number $M = u_\infty / a_0$, set to $M = 0.3$, with a_0 the speed of sound. The airfoil has a rounded trailing edge with radius

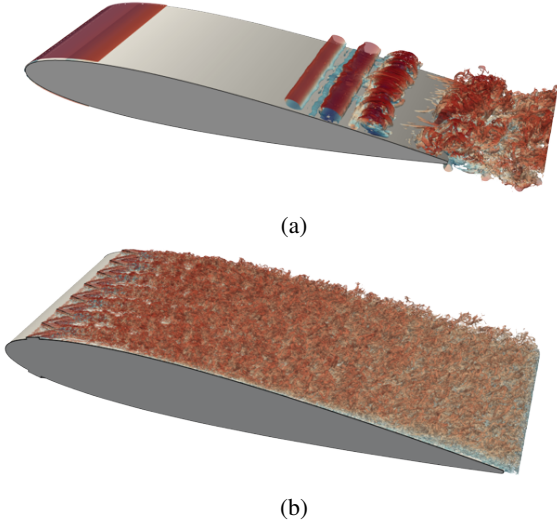


Figure 1: Iso-surfaces of the Q-criterion coloured by streamwise velocity for (a) the smooth airfoil at $Re = 5.10^4$ and (b) the tripped airfoil at $Re = 2.10^5$.

$r/c = 0.4\%$ and an angle of attack $\alpha = 3$ deg.

The first case considers a smooth surface airfoil at a Reynolds number of $Re = 5.10^4$, which results in tonal trailing-edge noise. The second case considers an airfoil with zigzag trips of height $h/c = 0.4\%$, located at $x/c = 5\%$ on both the suction and pressure sides. The Reynolds number is $Re = 2.10^5$, which results in broadband trailing-edge noise.

The datasets are obtained from compressible implicit LES, performed in the open source, high order flux-reconstruction, PYFR framework (Witherden *et al.*, 2014). Turbulent structures near the wall are resolved with mesh sizes corresponding to $\Delta y^+ < 1.0$, $\Delta x^+ < 5$, and $\Delta z^+ < 10$, with (x, y, z) respectively the streamwise, spanwise, and vertical directions. The numerical domains extends from -15 to 15 chordlengths along x and y , and spans 0.4 chordlength along z . Figure 1 shows iso-contours of the Q-criterion obtained from snapshots of each dataset.

The discrete set of equations obtained from the spatial discretization is integrated in time using an explicit fourth-order Runge-Kutta method. The simulations are performed on a cluster of Nvidia A100 GPUs.

3 Methodology

Resolvent analysis: The compressible Navier-Stokes equations are considered that describe the flow dynamics and acoustic field. The flow is described in terms of $q = [\rho, \mathbf{u}, p]^T$, with components referring to the density, velocity vector, and pressure, respectively. Additionally, the temperature T is substituted by the ideal gas equation of state and the molecular viscosity μ_m is obtained from the temperature via Sutherland’s law.

We model coherent structures with the resolvent method introduced by McKeon & Sharma (2010). First, the flow quantities in the governing equations are substituted by their triple decomposition (Reynolds & Hussain, 1972): $q = \bar{q} + \tilde{q} + q''$, where \bar{q} denotes the time-span average, \tilde{q} the coherent fluctuation, and q'' the stochastic fluctuations. Assuming the coherent structures to be periodic in time with an angular frequency ω , and in the spanwise direction with a wavenumber k_z , the system is solved in the frequency domain. Transport equations of the coherent fluctuations are obtained by subtract-

ing the mean from the phase-averaged equations, leading to

$$[\mathbf{A}(k_z, \bar{q}) - i\omega\mathbf{B}(\bar{q})] \tilde{q} = \tilde{f} \quad (1)$$

The nonlinear terms are lumped into the right-hand-side harmonic forcing term \tilde{f} , which includes the coherent Reynolds stresses $\widetilde{\mathbf{u}''\mathbf{u}''}$. This term is removed from \tilde{f} and modelled via a frozen eddy viscosity in a Boussinesq-like model

$$-\widetilde{\mathbf{u}''\mathbf{u}''} = \bar{\mu}_t \left[(\nabla + \nabla^T)\tilde{\mathbf{u}} - \frac{2}{3}\nabla \cdot \tilde{\mathbf{u}}\delta_{ij} \right]. \quad (2)$$

As a result, the viscosity appearing in the viscous tensor is defined as the sum of the molecular and eddy viscosities $\bar{\mu} = \bar{\mu}_m + \bar{\mu}_t$ in the final system. Resolvent analyses of turbulent channels (Symon *et al.*, 2023) have shown that considering an eddy viscosity could significantly improve the comparison with SPOD modes. In this work, a constant eddy viscosity as a first step, following Kuhn *et al.* (2021). A value of $\mu = 100/Re$ is selected for the broadband case, a posteriori, and the resulting setup is called *eddy* resolvent. In both the tonal and broadband case, results are computed with $\mu = 1/Re$, which is called *laminar* resolvent.

The resulting system in frequency domain is then written in an input-output form

$$\hat{q} = \mathcal{H}(\bar{q}, \omega, k_z)\tilde{f}, \quad (3)$$

where \mathcal{H} is the resolvent operator that linearly maps any arbitrary volume forcing \tilde{f} onto the response \hat{q} .

Orthogonal bases of pairs of forcings and responses, ranked in terms of energy gains are constructed from the singular value decomposition of the resolvent operator $\mathcal{H} = \sum_{j=1}^{\infty} \psi_j \sigma_j \phi_j^*$. The ϕ_j and ψ_j are respectively the forcing and response bases, related by the gains σ_j . In the case where $\sigma_1 \gg \sigma_2$, the flow dynamics are said to be “low-rank” and the response of the flow may be approximated with the optimal response ψ_1 alone. The resolvent analysis is performed using the Finite Element Linearized (Combustion) Solver FELiCS (Kaiser *et al.*, 2023), and we restrict our analysis to spanwise coherent structures ($k_z = 0$).

SPOD: SPOD is applied to the LES snapshots to extract the dominant coherent structures. The method extracts a set of orthogonal basis functions from the inner product of flow realisation in the frequency domain, defining an energy norm. The leading spatio-temporal coherent structures of the flow are then identified from the eigenvalue decomposition of the resulting operator (Schmidt *et al.*, 2018).

In the present work, the SPOD analysis is performed for the $k_z = 0$ fluctuations of pressure, which defines a p^2 -like energy. Since hydrodynamic fluctuations have a significantly larger amplitude than acoustic waves, this choice of norm still allows to extract similar coherent structures as if choosing a turbulent-kinetic energy norm. One practical advantage of using the pressure fluctuations is that the acoustic field associated with each SPOD mode is readily available.

Acoustic analogy: Curle’s acoustic analogy is used to approximate the far-field noise from surface pressure fluctuations, which is appropriate for an impenetrable surface S and a fixed airfoil position relative to the observer at \mathbf{x}_{obs} . In a two-dimensional domain, a free-field Green’s function for the convected wave equation can be used to derive the sound pressure at a specified observer point \hat{p}_{obs} in the frequency domain from

$$\hat{p}_{obs} = \int_{\partial S} \mathcal{C}(x_{obs}, x_s, \omega, M)\hat{p}_S dx_s, \quad (4)$$

where \mathcal{C} is a function including the terms from Curle’s solution accounting for mean-flow convection available in Sandberg & Sandham (2008). In this work, the input surface pres-

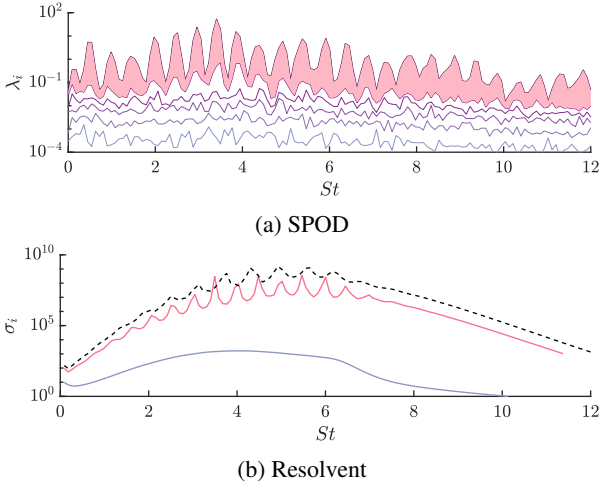


Figure 2: Spectra from (a) SPOD of LES snapshots and (b) the compressible resolvent. The leading gain from incompressible resolvent is added for comparison (---).

sure fluctuation is extracted from the leading SPOD and resolvent mode. An advantage of reconstructing the acoustics from an analogy instead of directly extracting them from the compressible LES or resolvent is that the former does not require high mesh density in the far-field to avoid numerical dissipation.

4 Tonal noise case

The first case presented in this paper is the smooth-surface airfoil at $Re = 5 \cdot 10^4$, which is known to result in tonal trailing-edge noise (Ricciardi, T.R. and Wolf, W.R. and Taira, K., 2022; Demange *et al.*, 2024).

The tones are directly observed in the SPOD spectrum shown in Fig. 2a, as the energy from the leading mode peaks at regular intervals of approximately $\Delta St \approx 0.5$. We note that the leading tone, with the highest energy, is found at $St = 3.4$. At the frequency of the tones, the large separation between the leading and sub-leading SPOD eigenvalues indicates a low-rank dynamic behaviour, which means that the leading SPOD captures most of the flow dynamics. The energy decay between first and sub-leading modes is less pronounced for frequencies in-between the tones, thus several modes may be needed to recover most of the dynamics at these frequencies.

Since the flow is not fully turbulent in the vicinity of the airfoil for the low-Re cas, the resolvent analysis is done only considering the molecular viscosity. Fig. 2b shows the gains from the two leading resolvent modes. Similarly to the incompressible analysis performed by the authors in a previous work (Demange *et al.*, 2024) for this case, a large gain separation is observed over most of the frequency range. Thus, the flow dynamics are low rank and only the leading resolvent mode is considered in the following.

In contrast to the incompressible analysis, peaks of the leading gain now match the frequency spacing from the SPOD, hinting that the compressible feedback mechanism underlying tonal trailing edge noise is captured by the linear operator. In contrast to the SPOD spectrum, the leading resolvent gain only displays tones for $2 \leq St \leq 7$, which suggest that higher and lower tones in the SPOD are harmonics of the main tones.

A comparison of the leading SPOD and resolvent modes is shown in terms of pressure fluctuations at the main tone frequency ($St = 3.4$) in Fig. 3. Both modes feature similar wavepackets on the suction side of the airfoil, near the trailing edge, which extend downstream in the wake. Acoustic waves

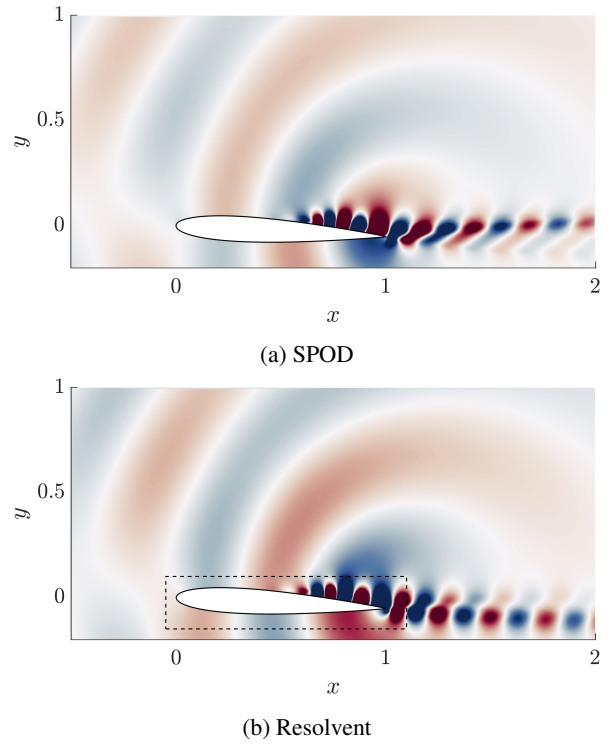


Figure 3: Pressure fluctuations obtained from (a) the leading SPOD and (b) resolvent modes at the main tone frequency ($St = 3.4$). The dashed rectangle in (b) indicates the region considered when computing the resolvent gains.

are also featured in both modes, with a good qualitative agreement. Discrepancies between the mode shapes are observed in the wake. Including an eddy viscosity in the resolvent could potentially address this difference, however, preliminary analyses did not reveal an improvement of the acoustic modelling when considering an eddy viscosity in this case.

The alignment between the leading SPOD and resolvent mode shape, defined as $\gamma_j = |\langle \bar{p}_i, \bar{p}_j \rangle| / (|\bar{p}_i| |\bar{p}_j|)$, is computed over the full range of frequency in order to further compare the resolvent to the data. The comparison, shown in Fig. 4, is done in term of surface pressure fluctuations only, since these are the only modal input required by the acoustic analogy to reconstruct the acoustic field.

Qualitatively, similar results than in the previously mentioned incompressible analysis are obtained when using the compressible formulation. An excellent alignment is observed for $1 < St < 7$, while the agreement of the resolvent with the SPOD deteriorates at lower and higher frequencies.

Finally, we compare the normalised directivity of the acoustic fields obtained from Curle’s analogy using either the SPOD or resolvent surface pressure fluctuations. Results are shown in Fig 5 for $St = [1, 3.4]$. The comparison shows an excellent agreement between the SPOD and resolvent at these frequencies, which extends to approximately $St \approx 8$, where the alignment also decreases significantly.

These results showcase that the compressible resolvent is a very good model for the trailing-edge noise for a significant portion of the frequency range. It is likely that higher-Strouhal tones are higher harmonics of the main dynamics, which cannot be captured by a linear mechanism.

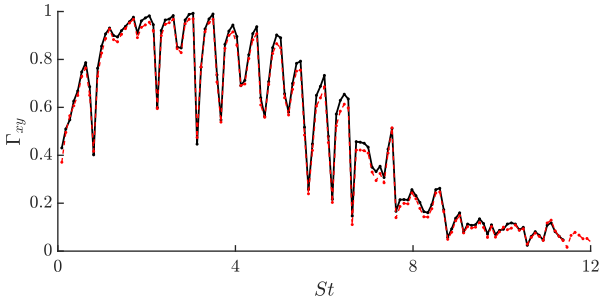


Figure 4: Alignment between the leading SPOD and compressible (black) incompressible (red) resolvent modes in terms of surface pressure fluctuations.

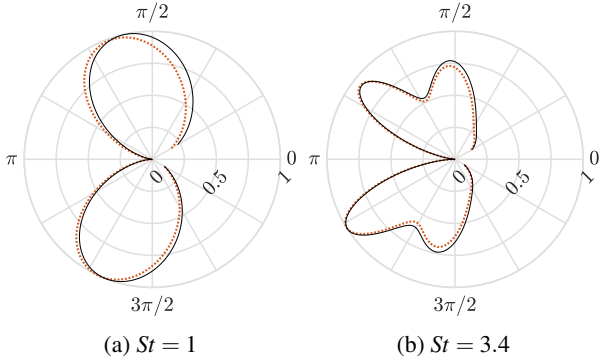


Figure 5: Normalised directivity of the acoustic fields obtained from the acoustic analogy based on the leading SPOD (---) and resolvent (—) modes at (a) $St = 1$ and (b) $St = 3.4$

5 Broadband noise case

A similar procedure is applied to the tonal case to investigate the airfoil with trip, featuring broadband noise. Since the mean flow is fully turbulent around the airfoil, the eddy viscosity is expected to have a greater influence on the results of the resolvent than in the tonal case. Thus, both the *eddy* and *laminar* versions of the resolvent are used.

Preliminary observations revealed that the trip used to trigger the turbulence was also found to emit acoustic waves, albeit mostly at high frequencies. Thus, in order to isolate trailing-edge noise, the SPOD considers a small domain on the suction side of the trailing edge to compute the energy of structures in the LES, shown in Fig. 7a. The full mode shape is then reconstructed by extended SPOD.

Fig. 6a shows the leading eigenvalues of the SPOD based on pressure fluctuations. The resulting spectrum is broadband, with the leading eigenvalue reaching its maximum at a Strouhal number of $St = 4.16$. A separation of about one order of magnitude is found between the leading and sub-leading eigenvalues for $St < 10$. Above this frequency, the dynamics become high-rank and the leading mode alone is no longer an appropriate representation of the flow dynamics. Instead, sub-leading modes should also be considered in this case, which is not attempted in this work and we will only consider $St \leq 12$.

The two leading resolvent gains are shown for both values of eddy viscosity in Fig. 6b. For the *eddy* resolvent ($\mu = 100/Re$), the gains are in very good qualitative agreement with the SPOD spectrum, showcasing low rank dynamics only for $St < 10$. However, the leading gain from the *laminar* resolvent ($\mu = 1/Re$) displays a peak around $St \approx 12$, which is not present in the SPOD. This peaks suppose the presence of a dis-

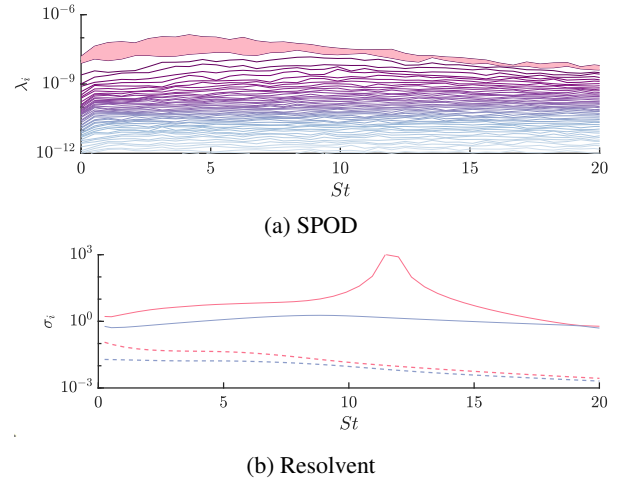


Figure 6: (a) SPOD spectra and (b) two leading gains from the *laminar* (—) and *eddy* (---) resolvent.

crete global mode close to the neutral axis in the linear operator at this frequency, which will be further discussed together with the mode shapes. Therefore, the addition of an eddy viscosity significantly improves the qualitative agreement between the resolvent gain curves with the SPOD eigenvalues, and the linear dynamics remain low rank for a frequency range similar to that of the SPOD with the *eddy* resolvent formulation.

The leading SPOD and resolvent mode shapes are shown in terms of pressure fluctuations in Fig 7 at the Strouhal number where the maximum energy was obtained in the SPOD ($St = 4.16$). The mode shapes from the SPOD and both resolvent formulations are in good qualitative agreement, displaying a wavepacket on the suction side of the trailing edge which extends in the wake, similarly to the tonal case. Similar acoustic waves are obtained for all modes. However, fluctuations close to the airfoil surface in the wake of the trips are observed in the SPOD but not in the resolvent. Although not plotted here, the first sub-leading resolvent mode also does not display these fluctuations. Further investigation is required to identify the causes of this discrepancy and its impact on the acoustic field.

Overall, the influence of the eddy viscosity on the resolvent mode is limited at this Strouhal number. The *laminar* resolvent displays a wave packet that extends slightly further upstream, while the *eddy* resolvent fluctuations in the wake dissipate faster. The influence of these slight variations on the acoustic fields will be discussed in more detail in the following.

The mode shapes of the two resolvent formulations and SPOD are further compared at $St = 12$ in Fig. 8, where a strong peak was observed only in the leading gain of the *laminar* resolvent. At his frequency too, both resolvent formulations (leading and sub-leading modes) miss the wavepackets in the wake of the trips, which now appears to have a larger amplitude relative to the trailing edge fluctuations in the SPOD.

However, at this Strouhal number, the influence of the eddy viscosity on the leading resolvent mode becomes more noticeable. On the one hand, the *laminar* resolvent displays a wavepacket confined to the near wake of the airfoil. This region features a small recirculation area in the mean flow velocity field, which further supports the hypothesis of a high-frequency global linear mode in this area when the influence of turbulent dissipation is neglected. On the other hand, the *eddy* resolvent displays a wavepacket further upstream of the trailing-edge, which is in very good agreement with the SPOD

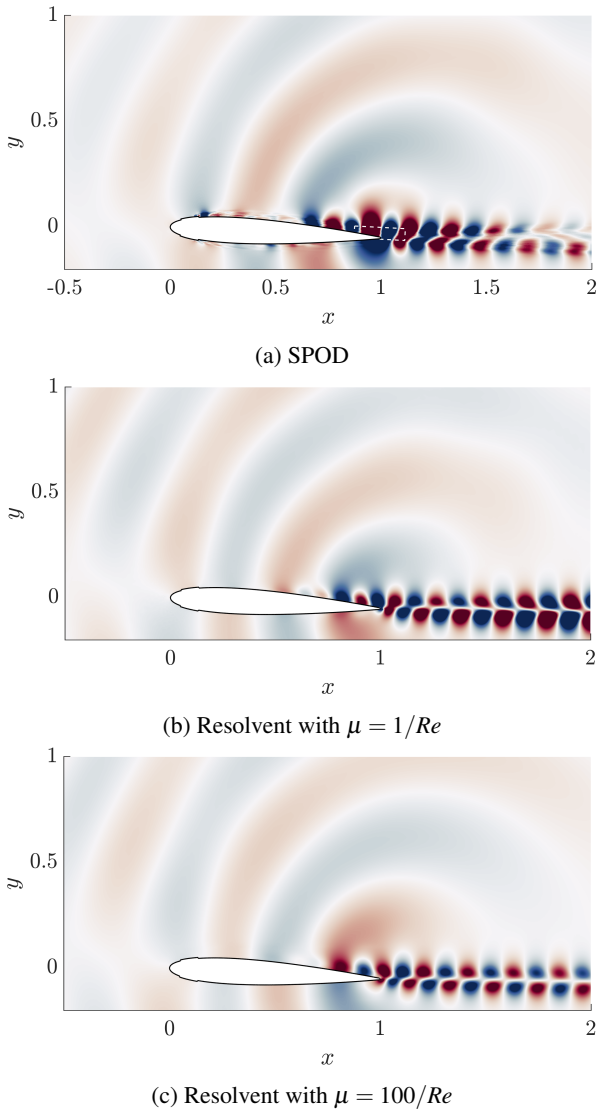


Figure 7: Leading mode shapes at $St = 4.16$, given in terms of pressure fluctuations from (a) the SPOD and from the resolvent assuming (b) $\mu = 1/Re$ and (c) $\mu = 100/Re$.

mode shape in this region, highlighting the importance of eddy viscosity on resolvent results based on turbulent mean flows. One should note, however, that the dynamics are high-rank at this frequency both in the SPOD and *eddy* resolvent, which implies that the leading mode alone is insufficient to reconstruct the acoustic field.

Similarly to the tonal case, the alignment between surface pressure fluctuations of the resolvent and SPOD modes is obtained over a wide frequency range, here extended to $St = 20$ for completeness. Results are shown in Fig. 9. For Strouhal number $St < 10$, when the dynamics are low rank, alignment values remain above 75% for both resolvent formulations, before decaying at higher Strouhal. At moderate Strouhal $St < 7$, the *laminar* resolvent gives slightly better results than the *eddy* one. However, the *eddy* resolvent mode performs better at higher Strouhal. Overall, these results show a very good match between the resolvent and SPOD when the system is low rank, and the current model of eddy viscosity seems to only improve the match between resolvent and SPOD in a given frequency range.

Finally, the normalised directivity from the leading modes of the SPOD and both resolvent formulations are shown in

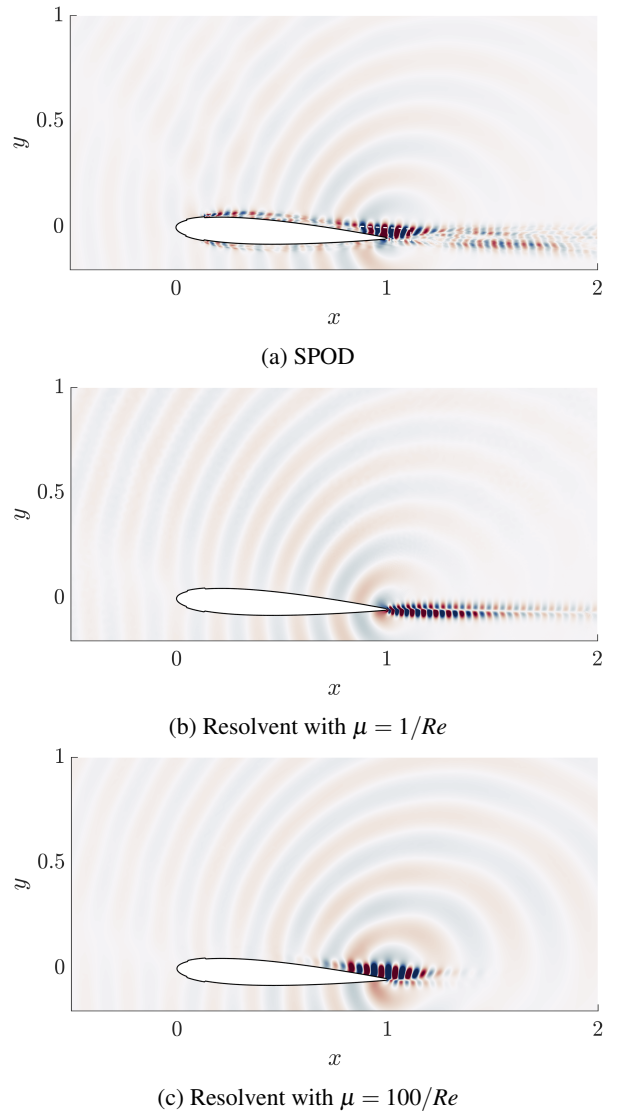


Figure 8: Same as Fig 7 but for $St = 12$.

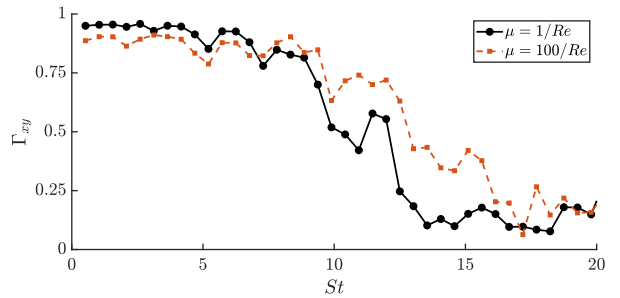


Figure 9: Alignment between the leading SPOD and resolvent modes in terms of surface pressure fluctuations.

Fig. 10, at Strouhal numbers where the dynamics are of low rank. For $St = 1$ and $St = 2$, the influence of the eddy viscosity on the directivity of the leading resolvent mode is negligible, and both formulations show a very good agreement with the leading SPOD mode. At $St \approx 4$, the SPOD acoustic fields exhibit three distinct lobes, which are partially recovered by the resolvent. At this frequency, the *eddy* resolvent performs better than the *laminar* one, despite having a slightly lower alignment with the SPOD surface pressure fluctuations. This result highlights the sensitivity of the directivity to small details of mode shapes, which may not always be evident from the alignment

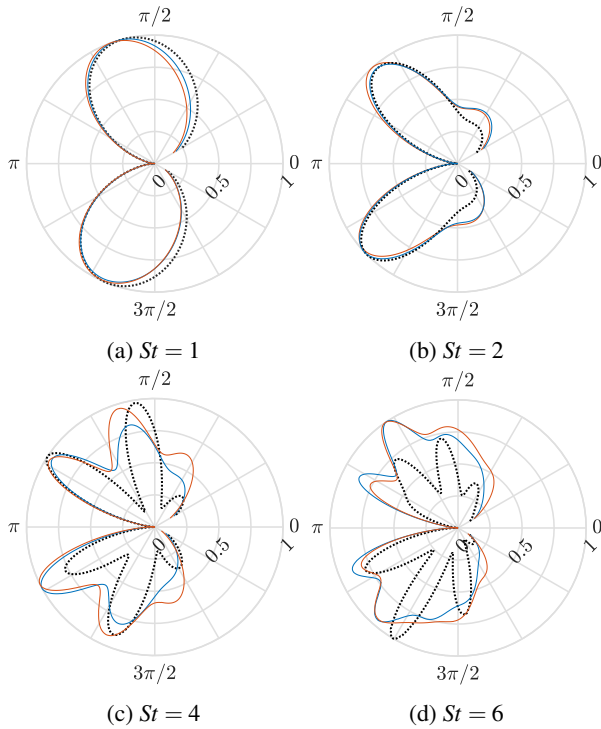


Figure 10: Normalised directivity of the acoustic fields obtained from the acoustic analogy based on the leading SPOD (\cdots) and resolvent with $\mu = 1/Re$ (blue —) and $\mu = 100/Re$ (red —) modes the resulting acoustic fields. Figures (a-d) correspond to $St = [1, 2, 4, 6]$ respectively.

measure alone. At higher Strouhal $St = 6$, only moderate qualitative agreement is obtained between the SPOD and the two resolvent formulations, despite the fact that the system is relatively low-rank at this frequency. Overall, the eddy resolvent analysis is in good agreement with the SPOD analysis at low to moderate Strouhal number, while discrepancies at higher Strouhal, potentially linked to the wavepackets generated by the trips, need to be investigated further.

6 Conclusions and outlooks

This work showed that compressible resolvent analysis can be used to model the trailing-edge (TE) noise radiated by a NACA0012 airfoil from the mean flow only. To highlight the versatility of this approach, the analysis was performed for two configurations resulting in either tonal or broadband TE noise. The SPOD of LES snapshots shows that, in both cases, TE noise is caused by a wavepacket on the suction side of the trailing edge for most of the frequency range studied.

A very good agreement is obtained between the leading SPOD and optimal resolvent mode shapes at low-to-moderate Strouhal numbers, which correspond to the range of low-rank dynamics identified in the SPOD eigenvalues. This range of frequency is relevant to TE noise as it corresponds to the highest sound levels for the cases investigated. In this regime, the directivity of the acoustic field from the resolvent matches well with that of the SPOD.

The role of eddy viscosity in resolvent analysis was investigated with a simple constant model for μ_t in the turbulent configuration. Including μ_t significantly improved the agreement between the trend of resolvent gain and SPOD eigenvalues, resulting in minor changes in the mode shapes at a moderate Strouhal number. However, even such slight changes were found to have a noticeable impact on sound directivity.

Thus, finding an appropriate eddy viscosity model is expected to yield further improvements in the TE noise model for turbulent cases.

This work has shown that, over a significant frequency range, TE noise is correlated to a simple dynamic structure. This finding has the potential to reduce the number of degrees of freedom in control and mitigation strategies for TE noise. Furthermore, the reported sensitivity of the acoustic directivity to small variations of the mode shape is promising for control purposes. Finally, since only the mean flow is required for the resolvent, a cheaper RANS-based approach could be considered.

REFERENCES

- Curle, N. 1955 The influence of solid boundaries upon aerodynamic sound. *Proc. R. Soc. Series A. Mathematical and Physical Sciences* **231** (1187), 505–514.
- Demange, S., Yuan, Z., Jekosch, S., Hanifi, A., Cavalieri, A.V.G., Sarradj, E., Kaiser, T.L. & Oberleithner, K. 2024 Resolvent model for aeroacoustics of trailing edge noise. *Theor. Comput. Fluid Dyn.*
- Kaiser, T.L., Demange, S., Müller, J.S., Knechtel, S. & Oberleithner, K. 2023 FELiCS: A Versatile Linearized Solver Addressing Dynamics in Multi-Physics Flows. In *AIAA AVIATION 2023 Forum*. San Diego, CA and Online: American Institute of Aeronautics and Astronautics.
- Kuhn, P., Soria, J. & Oberleithner, K. 2021 Linear modelling of self-similar jet turbulence. *J. Fluid Mech.* **919**, A7.
- Lee, S., Ayton, L., Bertagnolio, F., Moreau, S., Chong, T. P. & Joseph, P. 2021 Turbulent boundary layer trailing-edge noise: Theory, computation, experiment, and application. *Prog. Aerosp. Sci.* **126**, 100737.
- Lighthill, M. J. 1952 On sound generated aerodynamically I. General theory. *Proc. R. Soc. Series A. Mathematical and Physical Sciences* **211** (1107), 564–587.
- McKeon, B.J. & Sharma, A.S. 2010 A critical-layer framework for turbulent pipe flow. *J. Fluid Mech.* **658**, 336–382.
- Nogueira, P. A. S., Cavalieri, A. V.G. & Jordan, P. 2017 A model problem for sound radiation by an installed jet. *JSV* **391**, 95–115.
- Reynolds, W.C. & Hussain, A.K.M.F. 1972 The mechanics of an organized wave in turbulent shear flow. Part 3. Theoretical models and comparisons with experiments. *J. Fluid Mech.* **54** (2), 263–288.
- Ricciardi, T.R. and Wolf, W.R. and Taira, K. 2022 Transition, intermittency and phase interference effects in airfoil secondary tones and acoustic feedback loop. *J. Fluid Mech.* **937**, A23.
- Sandberg, R.D. & Sandham, N.D. 2008 Direct numerical simulation of turbulent flow past a trailing edge and the associated noise generation. *J. Fluid Mech.* **596**, 353–385.
- Schmidt, O.T., Towne, A., Rigas, G., Colonius, T. & Brès, G.A. 2018 Spectral analysis of jet turbulence. *J. Fluid Mech.* **855**, 953–982.
- Symon, S., Madhusudanan, A., Illingworth, S. J. & Marusic, I. 2023 Use of eddy viscosity in resolvent analysis of turbulent channel flow. *Phys. Rev. Fluids* **8** (6), 064601.
- Wagner, G. & Sandberg, R. 2020 Resolvent Method Surface Pressures for Airfoil Trailing-Edge Noise Prediction. In *22nd AFMC2020*. Brisbane, Australia.
- Witherden, F.D., Farrington, A.M. & Vincent, P.E. 2014 Pyfr: An open source framework for solving advection–diffusion type problems on streaming architectures using the flux reconstruction approach. *Comput. Phys. Commun.* **185** (11), 3028–3040.